Mol Neurobiol
DOI 10.1007/s12035-016-0369-2

Iron Availability Compromises Not Only Oligodendrocytes But Also Astrocytes and Microglial Cells

Maria Victoria Rosato-Siri[1] · Leandro Marziali[1] · María Eugenia Guitart[1] · Maria Elvira Badaracco[1] · Mariana Puntel[2] · Fernando Pitossi[2] · Jorge Correale[3] · Juana Maria Pasquini[1]

Received: 26 September 2016 / Accepted: 28 December 2016

Abstract When disrupted, iron homeostasis negatively impacts oligodendrocyte (OLG) differentiation and impairs myelination. To better understand myelin formation and OLG maturation, in vivo and in vitro studies were conducted to evaluate the effect of iron deficiency (ID) not only on OLG maturation but also on astrocytes (AST) and microglial cells (MG). In vivo experiments in an ID model were carried out to describe maturational events during OLG and AST development and the reactive profile of MG during myelination when iron availability is lower than normal. In turn, in vitro assays were conducted to explore proliferating and maturational states of each glial cell type derived from control or ID conditions. Studies targeted NG2, PDGFRα, CNPAse, CC1, and MBP expression in OLG, GFAP and S100 expression in AST, and CD11b, ED1, and cytokine expression in MG, as well as BrDU incorporation in the three cell types. Our results show that ID affected OLG development at early stages, not only reducing their maturation capacity but also increasing their proliferation and affecting their morphological complexity. AST ID proliferated more than control ones and were more immature, much like OLG. Cytokine expression in ID animals reflected an anti-inflammatory state which probably influenced OLG maturation. These results show that ID conditions alter all glial cells and may impact myelin formation, which could be regulated by a mechanism involving a cross talk between AST, MG, and oligodendrocyte progenitors (OPC).

Keywords Iron deficiency · Oligodendrocyte maturation · Astrocyte response · Microglial cell activation · Hypomyelination

Introduction

In humans, iron deficiency (ID) is a common nutritional condition whose consequences include neurological disorders and anemia [1, 2]. These findings suggest that iron acquisition during the prenatal and postnatal periods is indispensable for normal central nervous system (CNS) myelination. Oligodendrocytes (OLG), the primary myelinating and iron-containing cells in the CNS, require iron as a cofactor for enzymes involved in myelin production and maintenance [3], although the specific role of iron and its underlying mechanisms remain to be elucidated.

ID imposed on developing rats has proven to be a useful model to understand associated changes in myelin composition, including a lower relative content of cholesterol and proteolipid protein (PLP) [4]. Iron also takes part in energy production through higher rates of mitochondrial oxidative metabolism in OLG [5], and a correlation has been established between iron dyshomeostasis and neuropathogenesis [6]. Histochemical studies have shown that high iron concentrations in OLG play a particular role in myelin production [7, 8]. In addition, animals exposed to a gestational ID diet have exhibited hypomyelination [4], as ID conditions correlate with alterations in the OLG population [8, 9] both in size and myelinating capacity. In turn, the oligodendrocyte progenitor (OPC) subpopulation expands but shows poor maturation, with fewer mature OLG (m-OLG) in ID than in control conditions [10]. OLG iron deposits are also detected in macrophages and astrocytes (AST) in experimental

Jorge Correale and Juana Maria Pasquini are senior authors of this paper

✉ Juana Maria Pasquini
jpasquin@qb.ffyb.uba.ar

[1] Departamento de Química Biológica, Facultad de Farmacia y Bioquímica. IQUIFIB-CONICET, Universidad de Buenos Aires, Junín 956, C1113 Buenos Aires, Argentina

[2] Instituto Leloir - IIBBA-CONICET, Buenos Aires, Argentina

[3] Instituto de Investigaciones Neurológicas Dr. Raúl Carrea, FLENI, Buenos Aires, Argentina

Published online: 14 January 2017

autoimmune encephalomyelitis mice [11], which suggests that macrophages and glial cells other than OLG may participate in altered iron metabolism in this multiple sclerosis animal model.

ID hypomyelination might also be associated to alterations in AST and microglial cell (MG) functions, which in turn fail to support OPC maturation. AST provide iron to MG [12, 13] which participate in the expression of IL-1β and TNF-α [14, 15]. These cytokines could either act directly on OPC or stimulate AST for the production of growth factors taking part in OPC differentiation, such as FGF-2 and IGF-1 [16–18]. IL-1β can also induce TGF-α expression by AST, which could directly contribute to OPC differentiation [19, 20]. Considering bibliographical evidence available so far, the impaired maturation of ID OLG might be thought of as an intrinsic cell dysfunction or it may also reflect the unfavorable cell scenario in which OLG progress to a myelinating state. In addition, it is possible that ID also leads to functional alterations in MG. During the early postnatal period, MG are thought to be an iron source for OLG and have actually been described as iron capacitors [8], because they accumulate iron prior to myelination and then decrease iron content as OLG accumulate it [21, 22].

Our current in vivo and in vitro findings suggest that hypomyelination in ID animals could be explained not only by an arrested immature OLG subpopulation but also by deficiencies in other glial cells, particularly AST maturation and responsiveness and MG response and cytokine expression, which further prevent OLG maturation and myelin formation. Furthermore, our data reveal a blockade of MG pro-inflammatory profile in ID animals [23]. In vitro data showed that all glial cells derived from gestational ID pups exhibited long-lasting effects of iron deprivation and similar features characterized them in cultures. These observations are also in agreement with in vivo data showing ID persistent effects even after 2 weeks of normal diet restoration.

Materials and Methods

Animals

Animal protocols were approved by the Institutional Review Board at Universidad de Buenos Aires and were in accordance with the National Institutes of Health Guide for the Care and Use of Laboratory Animals. Wistar rats were housed under controlled temperature (22 ± 2°C) in an artificially lit animal room under a 12-h light/dark cycle and fed water and food ad libitum.

In Vivo Experimental Design

Pregnant Wistar rats were fed a normal diet (C; 40 mg Fe/kg) or an iron-deficient diet (ID; 4 mg Fe/kg) from gestational day five (E5) until weaning at postnatal day 21 (P21). After weaning, the offspring was fed a normal diet. The myelination process was delimited by two time points, P21 and P35. P21 represents an important transition point before the onset of puberty, which begins during the fourth week of age. Within our experimental protocol, this time point stands for the peak of the myelination process, while P35 represents the point of complete and steady myelination (Scheme 1, upper panel). Two-way analysis of variance (ANOVA) did not reveal significant sex-dependent differences for the parameters analyzed at the time points selected.

In Vitro Experimental Design

Total brains of P0–1 pups born to rats fed either a normal (C cultures) or an iron-deficient diet (ID cultures) were used for primary cultures following the method already described [24]. Brains were dissected and plated on T75 polylysinated flasks and cultured in Dulbecco's Modified Eagle's medium (DMEM) supplemented with F12 (DMEM/F12) supplemented with 10% FCS for 14 days. Following the original protocol, MG, OLG, and AST cells were sequentially obtained by differential centrifugation. MG and AST were cultured in DMEM/F12 and 10% FCS for 24 h. *media* were changed to DMEM/F12 1% FCS. MG C and MG ID were treated either with saline solution (SAL) or LPS (100 ng/ml) [25]. OLG cultures were maintained in a complete Glial Defined Medium (GDMc) for 24 h previous to any treatment; cultures were maintained up to 3 or 5*div*. Supernatants of AST cultures were assayed in OLG cultures (AST-conditioned medium) as compared to a nonconditioned (GDMc). Assays were performed adding equal volumes of GDMc 2× and the corresponding AST-conditioned supernatant. 5*div* OLG cultures were used to study differentiation effects. At 4*div*, AST C and AST ID were treated for 24 h either with SAL or H_2O_2 (50 μM) [26] (AST LPS- or H_2O_2-challenged, respectively). Cultures were fixed with 30 min methanol at −20°C, rinsed twice with PBS and stored at −20°C until used and analyzed by ICC and qRT-PCR techniques. Culture purity was checked using anti-O4, anti-CD11b, anti-NeuN, and anti-GFAP antibodies.

Brain Sections

P21 and P35 rats were anesthetized with a ketamine-xylazine mixture (75–10 mg/kg) and intracardiacally perfused with phosphate-buffered saline (PBS), pH 7.4, and ice-cold 4% *p*-formaldehyde (PFA). Brains were removed, postfixed overnight at 4°C and then processed as previously described [27].

Eriochrome Cyanine and Sudan Black Staining

Cryostat sections were stained according to Eriochrome cyanine [28] or Sudan black [29] protocols.

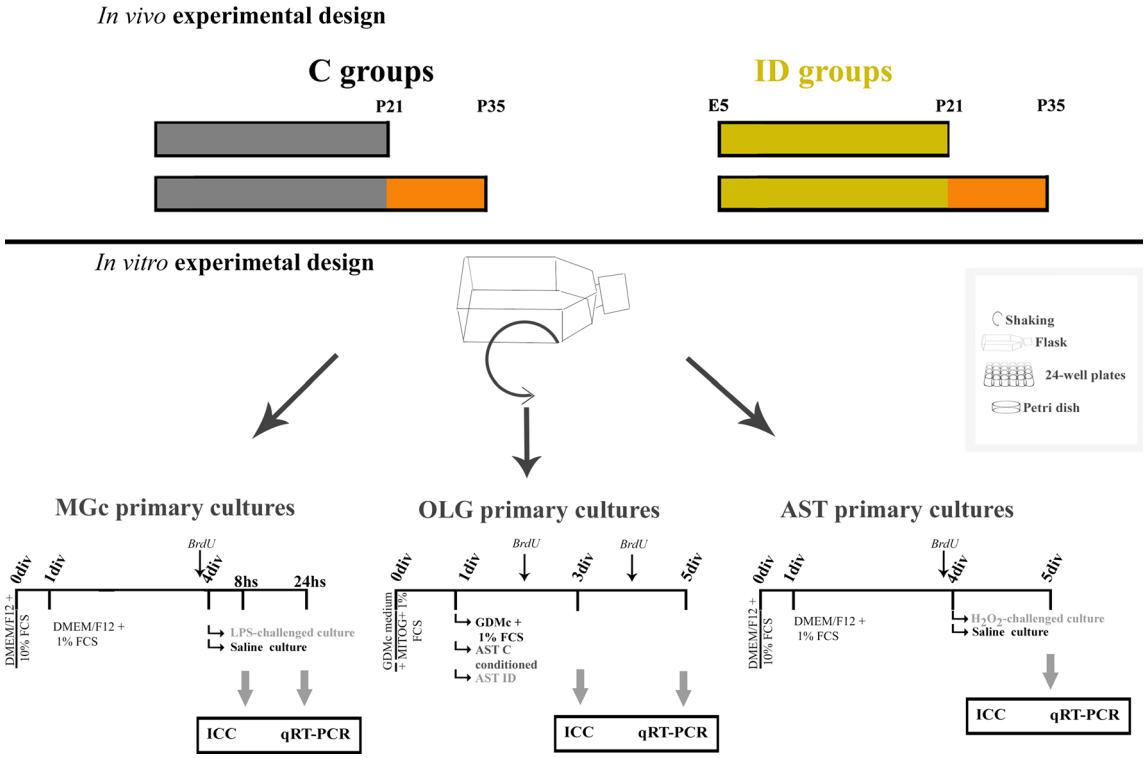

Scheme 1 In vivo and in vitro experimental design. *Gray bars* indicate the weaning period, during which pregnant rats were fed a normal diet (*C*), while yellow bars show iron deficiency diet (*ID*) (*upper panel*). *Orange bars* indicate that, after weaning, animals were fed a normal diet. For each experimental condition, siblings were sacrificed at P21 or P35; brains were then processed for IHC (n = 10) or qRT-PCR analyses (n = 6). Brains from P0–1 pups born to rats fed either a normal (C cultures) or an iron-deficient diet (ID cultures) were dissected and plated on T75 polylysinated flasks and cultured in DMEM/F12 supplemented with 10% FCS for 14 days (*lower panel*). MG, OLG, and AST were sequentially obtained as described in the original method. MG and AST were cultured in DMEM/F12 + 10% FCS for 24 *H. media* were changed to DMEM/F12 1% FCS. After 4*div*, MG C and MG ID were treated either with SAL or LPS and fixed at 6*div*. ICC assay: 6 × 103cells/well, on coverslips placed in a 24-well plate. qRT-PCR technique: 5 × 105cell/dish. OLG cultures were maintained in a complete GDMc medium for 24 h previous to any treatment. OLG were cultured either in a nonconditioned or in a conditioned medium (GDMc and supernatants of AST cultures, respectively). ICC assay: 2 × 103cells/well, on coverslips placed in 24-well plate. qRT-PCR technique: 5 × 105cell/dish At 4 *div*, AST C and AST ID were treated for 24 h either with SAL or H_2O_2. ICC assay: 5 × 104cells/well, on coverslips placed in a 24-well plate. qRT-PCR technique: 7.5 × 105cell/dish. BrdU pulses (white arrows) were supplied 24 h before fixation. Culture purity was checked using anti-O4, anti-CD11b, anti-NeuN, and anti-GFAP antibodies; n = 6 (independent cultures)

Immunodetection

Immunohistochemistry (IHC) and immunocytochemistry (ICC) were performed as described in [30]. Primary antibody specifications were OPC marker anti-NG2 (rabbit) 1:100 (Millipore, Temecula. CA, USA); OPC and pre-OLG (p-OLG) marker anti-PDGFRα (goat) 1:100 (Neuromics Antibodies, Edina, CA, USA); m-OLG markers anti-CC1/APC (mouse) 1:100 (Abcam, Cambridge, MA, USA) and anti-MBP (rabbit) 1:500, a gift from Dr. A. Campagnoni, UCLA; p-OLG to m-OLG, anti-O4 (mouse) 1:50, a gift from Dr. A. Campagnoni, UCLA. AST markers anti-GFAP (chicken) 1:500 (Neuromics Antibodies, Edina, CA, USA), anti-S100β (rabbit) 1:500 (Abcam, Cambridge, MA, USA) and anti-connexin 43 (CX43, rabbit) 1:400 (Invitrogen, Camarillo, CA, USA); MG markers anti-CD11b (mouse) 1:100 (Millipore, Temecula, CA, USA) and anti-ED1 (mouse) 1:100 (Abcam, Cambridge, MA, USA); proliferating state markers anti-BrdU (mouse) 1:500 (Roche, Mannheim, Germany) and anti-CXCR4 (mouse) 1:100 (RyD System, Minneapolis, MN, USA). Corresponding secondary antibodies were purchased from Jackson ImmunoResearch (West Grove, PA, USA) and were used in a 1:500 dilution (fluorescent-conjugated); Höechst dye was added together with the secondary antibody solution.

Quantification Strategies: Image ProPlus 5.1 was used throughout. Mean number of $CC1^+$ cells: CC1 immunoreactivity and $Höechst^+$ nuclei were quantified separately; enhancement contrasts were set to make sharp images of positive nuclei and two-spatial filtering was applied: enhancement (HiGauss; 5 × 5) and edge (variance; 5 × 5). A grid was used to divide each photograph and the number of nuclei intersecting the uppermost focal plane was counted (on-focus nuclei). Image operation tool "Add" was used to discriminate between the number of nuclei surrounded by CC1 immunoreactive cytoplasm and those devoid of $CC1^+$ reactivity [30]. The average MBP immunodetection was quantified by integrated optical density (IOD). Mean numbers of PDGFRα,

MBP, O4/ PDGFRα, O4/MBP, and $BrdU^+$ cells were determined using "area and aspect" plugins and "threshold" tool to determine "positive events."

BrdU Incorporation

BrdU (10 μM) was added at the beginning of each treatment and quantified at the corresponding end points (Scheme 1, lower panel, white arrows). Regarding OLG cultures, the design was chosen in order to establish the proliferative state of a particular cell population at a specific time point (3 and 5*div*). Therefore, some cells were both $NG2^+$ and $BrdU^+$, but no cells were both MBP^+ and $BrdU^+$.

Microscopy and Image Analysis

Digital images were acquired with an epifluorescence Olympus BX50 microscope equipped with a CoolSnap digital camera.

RNA Extraction and Quantitative RT-PCR

Brains from the four primary groups were dissected and the anterior and posterior regions of the corpus callosum (CC) were processed separately. RNA was extracted from samples using Trizol reagent following the manufacturer's instructions. cDNA synthesis was performed using 1 μg total RNA and Moloney Murine Leukemia Virus (M-MLV) reverse transcriptase according to the manufacturer's instructions (Promega, Madison, WI, USA). After retro-transcription, RNA was degraded and cDNA precipitated. Briefly, NaOH was added to a final concentration of 0.5 M, samples were incubated at 65°C for 30 min, HEPES solution was added to neutralize and cDNA was precipitated with ethanol. cDNA was quantified with the Quant-iT™ OliGreen® ssDNA Assay Kit following the manufacturer's instructions. Specific primer dynamic ranges were performed from 80 to 5 ng cDNA covering 1:2 serial dilutions. Ten nanograms cDNA was used for each PCR reaction (Stratagene Mx3005P qPCR System). PCRs were performed as follows: primers (0.4 μM of the corresponding pair), 1.25 U Platinum® Taq DNA polymerase, 0.3× SYBR® Green I Nucleic Acid Gel Stain, 0.05× ROX Reference Dye (Invitrogen, Camarillo, CA, USA), 0.3 mM dNTPs mix, and 4 mM $MgCl_2$. Cycling parameters: initial 4-min denaturation step at 94°C, sequential cycles of 30 s at 94°C, 30 s at 60°C, and 30 s at 72°C. Results were analyzed by the comparative CT method using Mx Pro–Mx3005P, v 4.10 associated software. The specific genes analyzed are summarized in Table 1.

Table 1 Specific genes analyzed

Gene	NCBI Ref. Sequence	Specific primers	
		Forward	Reverse
PDGFRα platelet-derived growth factor receptor alpha polypeptide	NM_012802.1	GCCACGAAAGAGGTCAAGGA	GCCTGATCTGGACGAAGCC
CNPase 2′,3′-cyclic nucleotide 3′ phosphodiesterase	NM_012809.2	CTACTTTGGCAAGAGACCTCC	AGAGATGGACAGTTTGAAGGC
GFAP glial fibrillary acidic protein	NM_017009	TGCAGGAGTACCAGGATCTAC	GGAGGTTGGAGAAAGTCTGTAC
S100β S100 calcium binding protein B	NM_013191.1	ATGTCTTCCATCAGTATTCAGGG	TCTCCATCACTTTGTCCACC
CXCL12 chemokine (C-X-C motif) ligand 12	NM_022177	CGCTCTGCATCAGTGACG	TGAAGGGCACAGTTTGGAGTG
CXCR4 chemokine (C-X-C motif) receptor 4	NM_022205.3	CCACAGAGTCAGAATCCTCAAG	GGTCAGCTCTTTATATCTGGGAAATG
Il-1β interleukin 1 beta	NM_031512.2	GGTGCTGATGTACCAGTTGG	TCCATGAGCTTTGTACAAGG
Il-10 interleukin 10	NM_012854.2	GACGCTGTCATCGATTTCTCC	CCAGTAGATGCCGGGTGGTT
TNF α Tumor necrosis factor alfa	NM_012675.3	GTAGCCCACGTCGTAGCAAA	AAATGGCAAATCGGCTGACG
IL-6 interleukin 6	NM_012589.2	CTCTCCGCAAGAGACTTCCAG	TCTGACAGTGCATCATCGCT
HPRT1 hypoxanthine phosphoribosyltransferase 1 (housekeeping gene)	NM_012583.2	TTCCTCCTCAGACCGCTTTTC	GGACTGAGGGTCGACATGACA
Tbp, 1–3 TATA box binding protein (housekeeping gene)	XM_006227980.2XM_008758748.1 XM_008758747.1	ACCGTGAATCTTGGCTGTAA	CCGTGGCTCTCTTATTCTCA

Target gene expression was quantified comparing its efficiency with that of the housekeeping gene [31].

OLG Morphology Analysis

The immature OLG stage was selected by PDGFRα immunodetection in C and ID cultures. Branching complexity was evaluated using Sholl analysis [32] and Sholl analysis plugin for ImageJ was used following Ferreira et al. [33]. The analysis of concentric circles around the cell body of PDGFRα$^+$ cells rendered five successive rings. The number of intersections of OLG processes and each ring was then counted. In particular, primary branches were inferred from their number in the starting ring. m-OLG were chosen as MBP$^+$ cells. Myelin-like membrane sheaths were outlined in ImageJ and the surface area quantified.

Statistical Analysis

For each in vivo experimental group, $n = 16$ (4 animals from four different litters). For in vitro experiments, $n = 6$ (independent cultures). The corresponding number of animals per treatment and replicates for consistency is indicated in each figure legend. Data were subjected to nonparametric tests suitable for normally distributed populations. Statistical analysis was performed using one-way ANOVA followed by different post-tests (GraphPad Prism, GraphPad Software Inc., La Jolla, CA, USA) or *t* tests when two groups were compared. *p* values of the different analyses are provided in the figure legends.

Results

Effects of ID on Myelin, OLG, and AST Differentiation and MG Activation in Vivo

At P21, Sudan black and Eriochrome staining analyses showed marked hypomyelination in the CC of the ID group (Fig. 1a, b), while CC1 IHQ revealed not only a significantly lower number of m-OLG but also changes in their distribution pattern when compared to the C group (Fig. 1d, c, respectively). The characteristic row pattern of consecutive nuclei within the CC was altered in ID animals (Fig. 1c and d, high magnifications, white lines), as visualized by shorter CC1$^+$ cell rows or cell gaps among m-OLG (Fig. 1, high magnifications, white arrows), which suggests that the effects of nutritional ID on brain iron metabolism are tightly associated with brain development. At P35, Sudan black and Eriochrome staining in C and ID animals confirmed the long-lasting effects of ID on myelin content even after 2 weeks of normal diet reinstatement (Fig. 2a). Specific OLG markers (Fig. 2b) [34] were evaluated to elucidate ID impact on different stages along the OLG lineage. qRT-PCR analyses of PDGFRα expression reflected an increase in the OPC/p-OLG subpopulations in ID animals as compared to C (Fig. 2c, upper panel). In contrast, CNPAse relative expression was significantly lower in ID than in C (Fig. 2c, lower panel). MBP IHQ showed similar results regarding abnormal myelin deposition, which leads to a hypomyelinated state in ID animals as compared to the C group (Fig. 2d). ID exhibited fewer cells with CC1$^+$ immunoreactivity when compared to C (Fig. 2e), revealing a smaller m-OLG subpopulation size.

The MG conditions associated with myelination progress were evaluated and the basal expression levels of IL-1β and IL-10 quantified by qRT-PCR. The CC of C and ID animals were dissected at P21and, in agreement with data reported in untreated mice [35], neither M1- nor M2-like phenotypes were exclusively present in C animals. ID animals showed no changes in IL-1β expression levels but a significant increment in IL-10 expression (Fig. 3a, left panel). In addition, the IL- 1β/IL-10 ratio showed a shift to an anti-inflammatory profile in ID animals, with values closer to 1 representing an increment in IL-10 relative expression (Fig. 3a, right panel). At P35, C and ID animals exhibited similar CD11b$^+$ cell IHQ (Fig. 3b), although they differed in the morphology of positive cells, with bulky cell bodies and shorter and thicker ramifications in ID animals (Fig. 3b, arrowheads) and a ramified shape in C animals (Fig. 3b, arrows). ED1$^+$ cell scattering confirmed the presence of activated MG in ID animals, in contrast with the C group, which rendered no ED1 IHQ (data not shown).

At P35, GFAP IHQ and its mRNA expression levels quantified by qRT-PCR showed a decrease in ID animals as compared to C (Fig. 4a, b, right panel, respectively). This decrease correlated with an increase in S100β expression levels (Fig. 4b, left panel).

Effects of ID on Glial Cell Proliferation and Differentiation in Vitro

As our in vivo findings indicate an arrest in OLG differentiation, subsequent studies were carried out on ID effects on proliferation. Previous studies demonstrate that, during ontogenetic myelination, OLG ID exhibit intrinsic alterations in terms of proliferation and migration. In addition, systemic BrdU supply renders a larger BrdU$^+$ subpopulation with an anomalous allocation within de CC of ID animals [10]. The present in vitro assays do not only confirm in vivo data but also expand them. As BrdU incorporation takes place only during a proliferative state, a pulse of BrdU was administered 24 h before fixation to evaluate proliferation at 3*div* and the enduring condition at 5*div*. In addition, different markers within the OLG lineage were used to establish the maturational state reached by the former proliferative cell (Fig. 5a). ICC analyses revealed that proliferating cells in ID cultures were mostly committed to the OLG lineage, as evidenced by NG2$^+$ immunostaining (Fig. 5b). PDGFRα mRNA expression

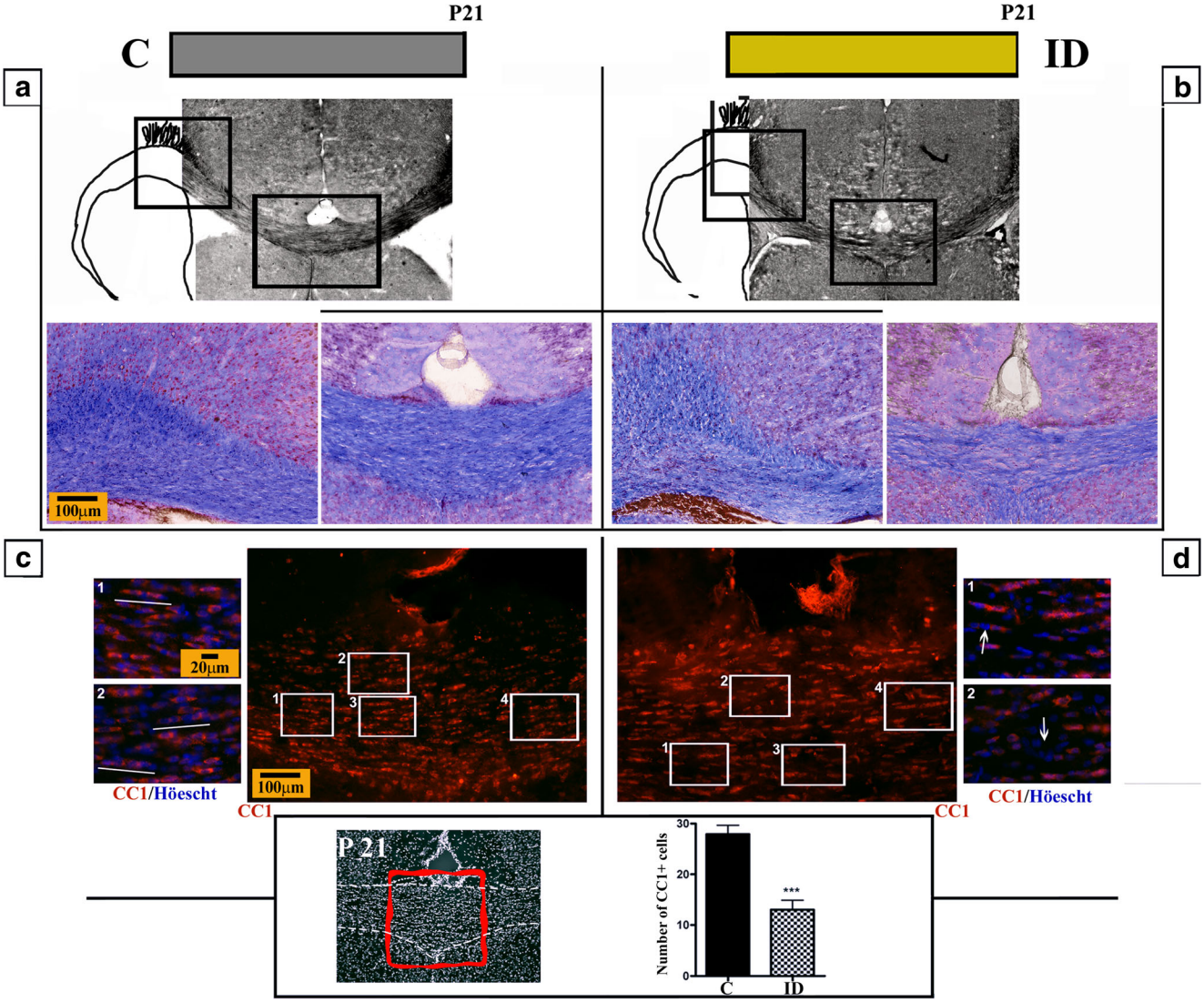

Fig. 1 Myelin and mature OLG at P21. **a**, **b** Brain coronal sections of the CC of C and ID animals, respectively, stained with Sudan black (*upper panels*) or Eriochrome cyanine R solution (*lower panels*). Images of the lateral (*left frame*) and medial part (*central frame*) of CC. **c**, **d** CC1 IHQ of C and ID animals, respectively. $CC1^+$ cells quantified using the procedure described in Fig. 4. Image operation tool "Add" was used to discriminate between the number of nuclei surrounded by CC1 immunoreactive cytoplasm and those devoid of CC1 reactivity. Quantification of nuclei surrounded by CC1-immunoreactive cytoplasm (*lower panel*). Significant differences found between groups (***$p < 0.001$) through *t* test. Scheme shows image location in a representative CC section. $n = 10$ animals, 4 slices of each animal, 4 randomly selected counting frames of 0.1 mm^2/slice. Frames 1–4 show high magnifications of central images

levels, characteristic of OPC and p-OLG, were found to be higher in OLG ID than in OLG C after 3*div*. After 5*div*, OLG ID maintained increased PDGFRα mRNA levels, while OLG C cultures showed an expected decrease (Fig. 5c). Cell morphology analyses using $PDGFR\alpha^+$ cells at *3div* to measure branching complexity (Fig. 5d) and primary branching (Fig. 5e) demonstrated an increased number of branching points and a larger total process surface in OLG ID. In ID cultures at *5div*, m-OLG showed a reduction not only in complexity, assessed by a diminished MBP^+ membrane area (Fig. 6a), but also in the percentage of positive cells (Fig. 6b). At the same time, OLG C exhibited an increase in the percentage of cells expressing this mature marker at the expense of an immature one (Fig. 6b). Altogether, these results indicate that cultured OLG ID maintained an immature profile, characterized by an increase in the number and complexity of OPC/p-OLG ($PDGFR\alpha^+$) cells and a decrease in m-OLG (MBP^+ cells). The in vitro experiments in the present work show that, in primary cultures kept in normal iron conditions, cells obtained from gestational iron deprivation pups exhibited long-lasting ID effects. In this case, the increase in proliferation probably reflects a compensation mechanism in which the shortage in m-OLG is made up for with an increase in the subpopulation which is supposed to mature (OPC/p-OL).

Preliminary experiments showed that the fresh supernatant of AST ID cultures used as conditioned media for 5*div* OLG C and OLG ID cultures did not alter m-OLG proportions as

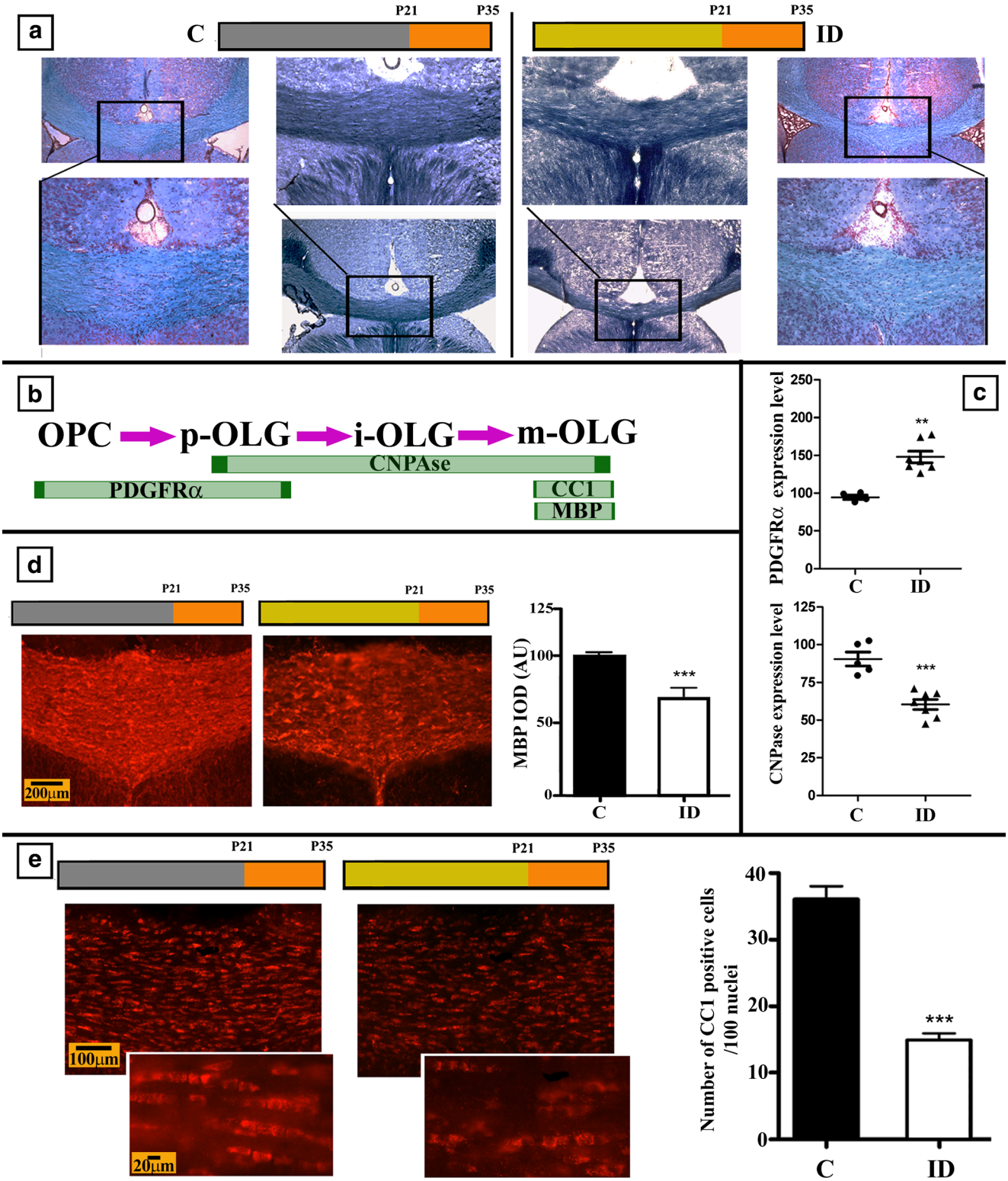

Fig. 2 Myelin and mature and immature OLG at P35. **a** Brain coronal sections of the CC of C and ID animals stained with Sudan black (*central images*) or Eriochrome cyanine R solution (*lateral images*). **b** Different OLG markers evaluated either by qRT-PCR or IHC: PDGFRα, marker of OPC and p-OLG; CNPase, marker of p-OLG, immature OLG and m-OLG; CC1 and MBP, exclusive markers of m-OLG. **c** Expression levels of PDGFRα and CNPase evaluated by qRT-PCR; values calculated relative to the housekeeping gene; $n = 6$. **d**, **e** Brain coronal sections from C and ID animals assessed for MBP immunoreactivity and $CC1^+$ cells. MBP quantitation expressed as average IOD (mean ± SEM; arbitrary units, AU). $CC1^+$ cells expressed as mean number/100 nuclei. Significant differences found regarding C (***$p < 0.001$; **$p < 0.01$; *ns* nonsignificant) through *t* test. $n = 10$. Replicates and counting frames as in Fig. 1

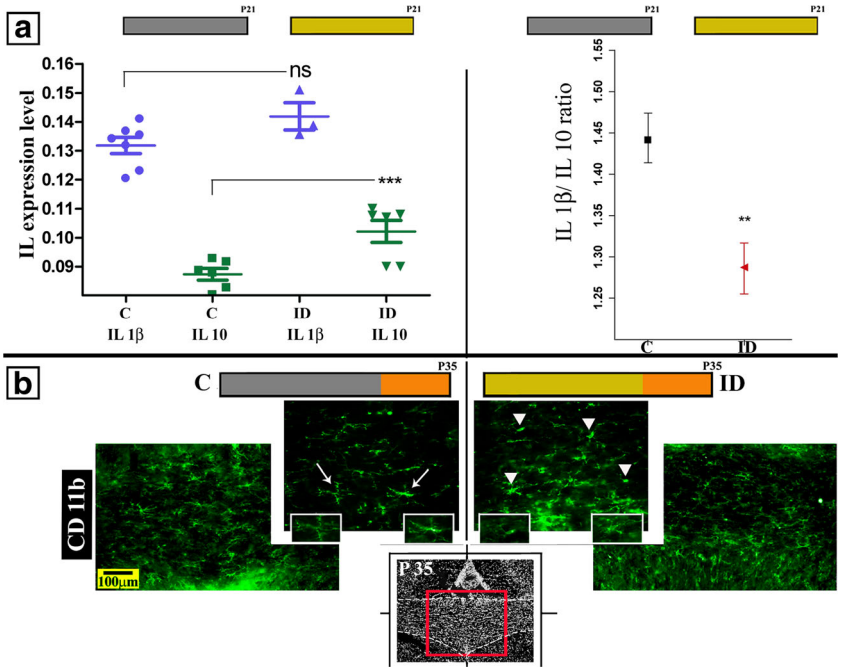

Fig. 3 Characterization of MG at P21 and P35. **a** Expression levels of IL-1β and IL-10 (*left panel*) and IL-1β/IL-10 ratio (*right panel*) evaluated by qRT-PCR at P21 Significant differences found regarding C (***$p < 0.001$; **$p < 0.01$; *ns* nonsignificant) through *t* test. **b** CD11b IHQ at P35 basal status; resting MG (ramified shape, *arrows*) and activated MG (bulky cells, *arrowheads* and *insets*)

compared to nonconditioned medium (Fig. 6c). In contrast, AST C conditioned media significantly reversed the immature state characteristic of OLG ID in vitro, increasing m-OLG percentage at the expense of immature OLG (Fig. 6c).

Further analyses showed that, after 5*div*, MG-C-LPS showed a slightly higher number of $BrdU^+$ cells as compared to C-MG-SAL after 8 h (22.6 ± 3.3 and 13.4 ± 2.4, respectively), with a wider gap 24 h later (81.5 ± 3.6 and 19.9 ± 2.9, respectively). In turn, MG ID showed similar values between 8-h SAL and 8-h LPS incubations (11.9 ± 1.3 and 20.3 ± 3.1, respectively). Although the number of $BrdU^+$ cells was higher 24 h later (61.6 ± 2.7), MG-ID-LPS exhibited a poor proliferation rate, as evidenced by a flattened slope (Fig. 7a). Cytokine expression levels quantified by qRT-PCR rendered, after 8-h LPS, an increase in IL-1β and TNFα in MG C as compared to MG-C-SAL and no changes in IL-10 or IL-6 (Fig. 7b). Worth highlighting, and in agreement with in vivo findings, no significant differences were observed between basal culture conditions MG-C-SAL and MG-ID-SAL. In addition, ID treatment offsets the LPS-mediated increase in IL-1β (Fig. 7b, left panel) and generated an increase in IL-10 levels (Fig. 7b, right panel). Regarding the evaluation of AST in basal and activated conditions, AST ID exhibited a long-lasting proliferating status, as evaluated by BrdU

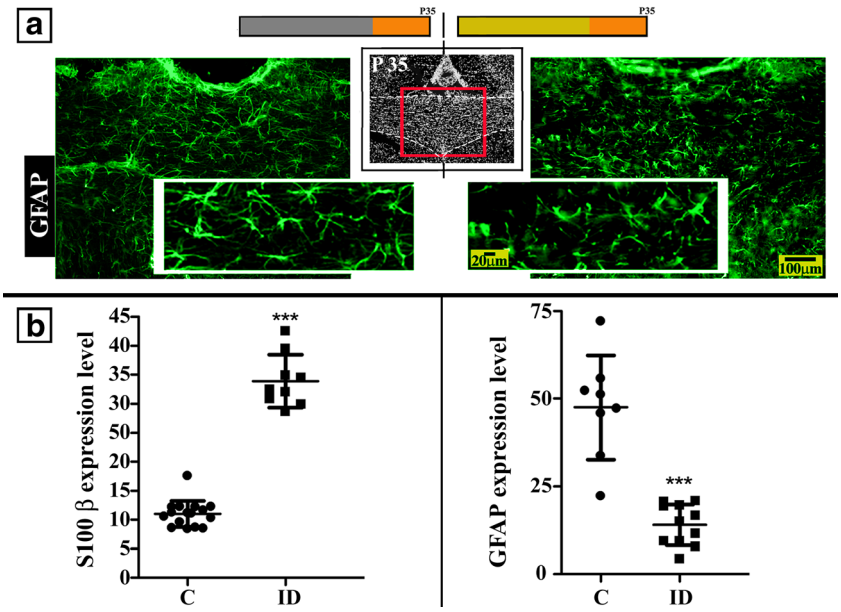

Fig. 4 Characterization of AST at P35. **a** GFAP IHQ in C and ID rats. **b** GFAP and S100β expression levels quantified by qRT-PCR in basal conditions in C and ID animals. Significant differences found between groups (***$p < 0.001$) through *t* test. Replicates and counting frames as in Fig. 1; the framed image shows the amplified CC region in each group

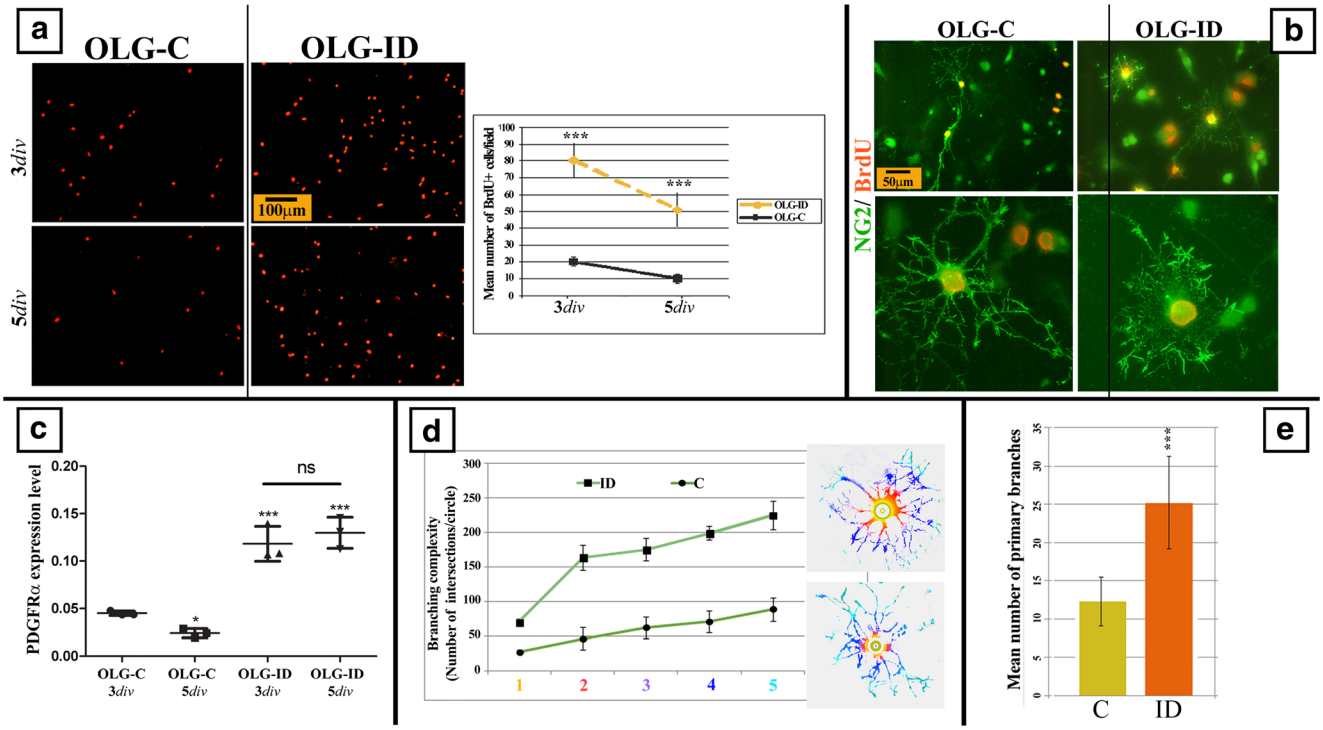

Fig. 5 Primary OLG cultures. **a** OLG were cultured for 3*div* and 5*div*, BrdU was added 24 h before fixation and BrdU$^+$ cells were quantified in OLG C and OLG ID cultures. Significant differences found between groups (***$p < 0.001$) through *t* test. **b** NG2 used as marker for neural precursor in OLG C and OLG ID cultures. **c** PDGFRα used as a marker of OPC and p-OLG quantified by qRT-PCR in C and ID cultures. Significant differences found regarding control condition (***$p < 0.001$; *$p < 0.05$; *ns* nonsignificant) through Newman-Keuls multiple comparisons posttest. **d** Branching complexity evaluated by Sholl analysis; the *X*-axis represents the circles around the cell body of PDGFRα$^+$ cells in C and ID cultures. **e** Primary branches were inferred from the number of process intersections with the starting circle. Significant differences found between groups (***$p < 0.001$) through *t* test

incorporation. This phenomenon was associated with an immature stage, which correlated with a decrease in CX43 expression (Fig. 8a) [36]. AST cultured at high density were also used to evaluate GFAP and S100β profiles, AST C showed a higher relative basal level of GFAP than AST-ID-SAL (Fig. 8b, arrows). In contrast, AST-ID-SAL showed an increase in S100β expression at the expense of GFAP (Fig. 8b, upper left panel, arrowheads). AST C response to H_2O_2 was characterized by a shift in marker expression, as evidenced by an increase in S100β and a decrease in GFAP ICC (Fig. 8b, lower left panel, arrowheads). This shift was not evident in AST-ID-H_2O_2, which exhibited the same expression profile of basal conditions (Fig. 8b, lower right panel, arrowheads). qRT-PCR assays provided support for ICC observations, as GFAP expression levels were significantly lower in AST ID than in AST C in basal conditions (Fig. 8c, left panel). AST exposure to H_2O_2 correlated with a shift to a reactive phenotype in C but not in ID cultures (Fig. 8c, middle panel). The decrease in the GFAP/S100β ratio reflected this transition in AST-C-H_2O_2 as compared to AST-C-SAL. The flat slope of AST ID accounts for a nonresponsive status (Fig. 8c, right panel).

In vitro data clearly showed that OLG, AST, and MG derived from gestational ID pups exhibited long-lasting effects of iron deprivation, as particular features characterized the three glial cell ID cultures, even in iron-sufficient medium. These observations remarkably resemble in vivo data, which proved that ID effects were evident even after 2 weeks of normal diet restoration.

Discussion

CNS development can be disrupted by several micronutrient gestational deficiencies, among which ID appears as the most prevalent. Furthermore, substantial damage derived from this gestational deficit cannot actually be reversed by later postnatal normal diet reinstatement, which reveals a possibly critical window of vulnerability during early development [37–40]. ID leads to hypomyelination both in animal models and humans, with significant neurological sequelae [4, 39, 41–44]. In this context, understanding the role of iron in myelination and OLG iron acquisition mechanisms and timing is necessary for effective intervention strategies.

Focusing on development, the present work employed an ID model which exhibited increased proliferation, altered morphology, augmented PDGFRα expression, and impaired OLG maturation when compared to control. At early stages of

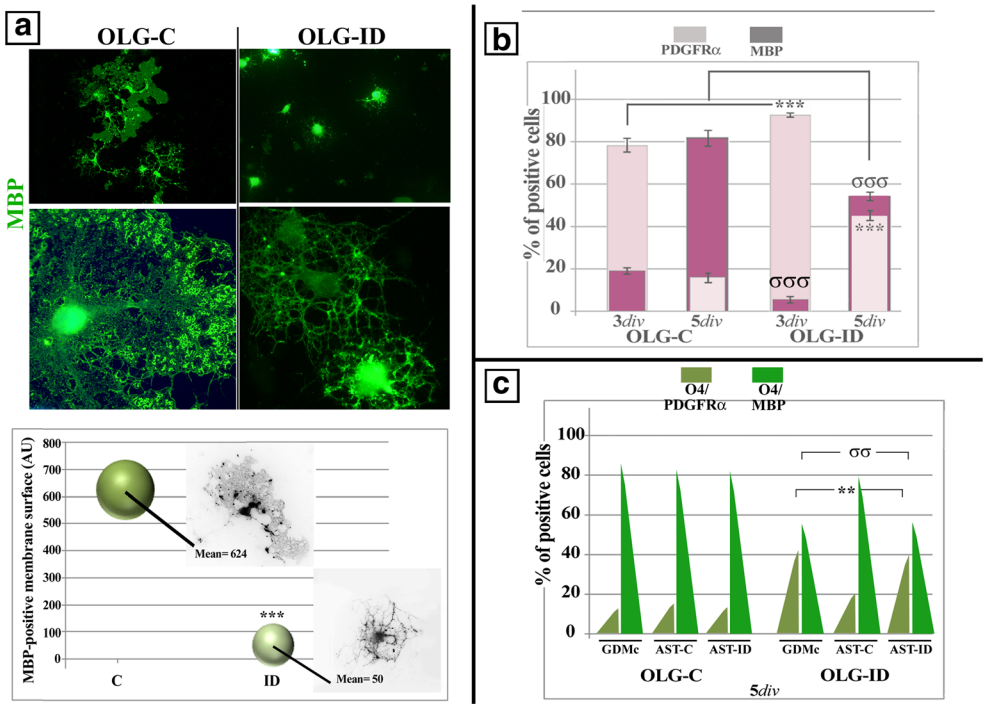

Fig. 6 OLG cytoarchitecture. **a** m-OLG were chosen by MBP$^+$ ICC. Myelin-like membrane sheaths, MBP$^+$, were outlined and their surface area quantified. Significant differences found between groups (***$p < 0.001$) through *t* test. **b** percentage of PDGFRα$^+$ or MBP$^+$ cells at 3*div* and 5*div* in C and ID cultures. Significant differences found regarding the corresponding control condition (for PDGFRα: ***$p < 0.001$; *$p < 0.05$; for MBP: σσσ $p < 0.001$; *ns* nonsignificant) through Newman-Keuls multiple comparisons posttest. **c** 5*div* OLG C and OLG ID were cultured either a nonconditioned medium (GDMc) or a conditioned one (AST C and AST ID). The percentage of double positive cells (O4/PDGFRα or O4/MBP) was determined. Significant differences found regarding OLG ID cultures (for O4/PDGFRα: **$p < 0.01$; for MBP: σσ $p < 0.01$) through Newman-Keuls multiple comparisons posttest

development, previous work by our group has already shown the relative amount of proliferating PCNA$^+$ cells to be slightly higher in ID than in controls [45]. In addition, the population of double positive cells (PCNA$^+$/Olig1$^+$ or PCNA$^+$/O4$^+$) is also larger in ID conditions, which indicates that most PCNA$^+$ cells remain in an undifferentiated state. These results suggest that the availability of precursors is higher in ID groups, in agreement with studies showing pregnancy ID to affect iron levels in the brain of developing fetuses, disrupting not only the proliferation of glial precursor cells but also disturbing the generation of OLG from these precursors [46]. In addition, Eriochrome cyanine assays in the present report provide evidence of low brain iron levels in ID animals, in agreement with recent studies on this technique [47].

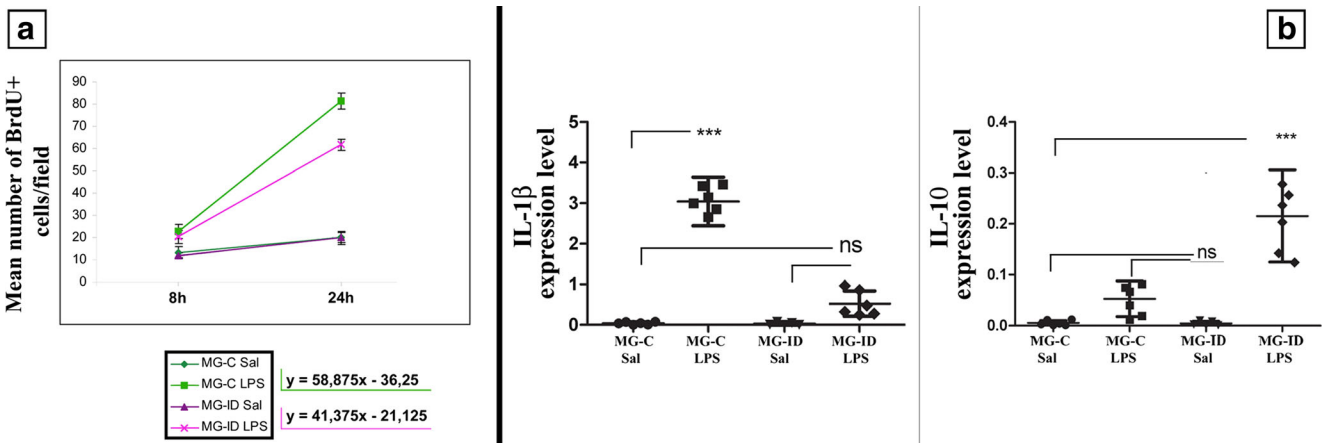

Fig. 7 Primary MG cultures. **a** MG were cultured for 4*div*, BrdU was added at the beginning of each condition (SAL or LPS) and evaluated 8 h and 24 h later. Linear regressions show MG C and MG ID kinetic responses to LPS culture conditions. **b** MG response profile evaluated by cytokine expression levels quantified by qRT-PCR. Significant differences found regarding MG-C-SAL (***$p < 0.001$; *$p < 0.05$; *ns* nonsignificant) through Newman-Keuls multiple comparisons posttest

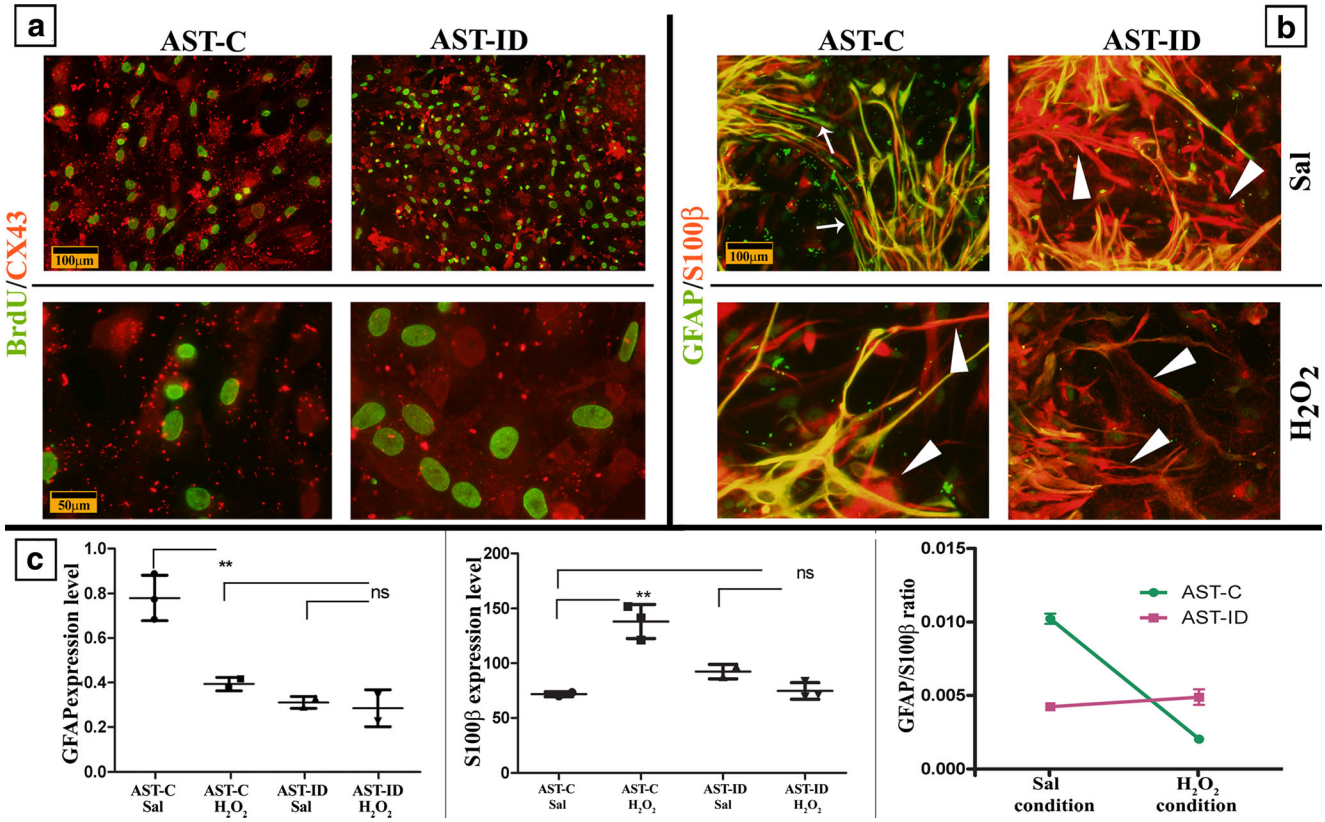

Fig. 8 Primary AST cultures. **a** AST were cultured for 5*div*, BrdU was added 24 h before fixation, and CX43 ICC was evaluated in AST C and AST ID cultures. **b** Culture challenge at 4*div* with H_2O_2 during 24 h; double ICC of GFAP/S100β. **c** GFAP and S100β expression levels quantified by qRT-PCR in basal and challenged conditions. AST response calculated through GFAP/ S100β ratio. Significant differences found regarding AST-C-Sal (**$p < 0.01$; *ns* nonsignificant) through Newman-Keuls multiple comparisons posttest

Numerous studies demonstrate the importance of the redox state as a regulator of the balance between self-renewing division and differentiation. One of these studies has shown that progenitors from the optic nerve myelinate relatively early and are intrinsically responsive to the induction of differentiation, which appears to be partly regulated by intra-cellular redox state [48]. Accordingly, our current work shows cells in ID conditions to exhibit a reduced redox state, as ID cultures were nonresponsive to H_2O_2. In addition, the characteristic row pattern of consecutive nuclei within the CC was altered in ID animals, as visualized by shorter $CC1^+$ cell rows in m-OLG. These findings support the notion that nutritional ID effects on brain iron metabolism are tightly associated with brain development.

Iron availability has been recently reported to exert a wide range of effects on glial cells other than OLG, both during development and as a response to injury [12, 19, 49–51]. It is well-known that AST influence OLG maturation through the secretion of different growth factors and actively contribute to efficient OLG differentiation [52]. AST have also been shown to capture circulating iron and distribute it to other cells via iron transporter ferroportin [53]. The induction of lysophosphatidylcholine-driven demyelination in ferroportin-knockout mice produces a clear decrease in the rate of remyelination through different mechanisms [19]. In addition, iron retention in AST could affect their activation state and cytokine secretion. Cytokines such as TNF-α and IL-1β have been shown to play a direct role in remyelination [17, 54] and to exert indirect effects by activating other cells within the CNS to produce growth factors involved in OPC proliferation and differentiation, such as IGF-1 and FGF-2 [17, 54, 55]. In contrast, increased iron availability in the CNS at early stages of development results in significantly increased AST GFAP expression levels [56].

In our ID model, AST remained in a clearly immature phenotype, as evidenced by a significant increase in proliferation, a decrease in CX43 expression and lower GFAP expression at the expense of S100β, both in vivo and in vitro. Hindered AST ID ability to mature could in turn affect the regulation of OLG differentiation and maturation, thus hampering proper myelination. Interestingly, reactive AST display a rapid upregulation of CX43, indicating an important role for the astrocytic response to injury [57], and exogenous iron increases CX43 expression and phosphorylation in enterocytes [58]. Overall, these observations support the notion that iron availability modulates CX43 expression and may consequently influence AST proliferation, migration, and differentiation [57], which in turn affects OLG. And, as

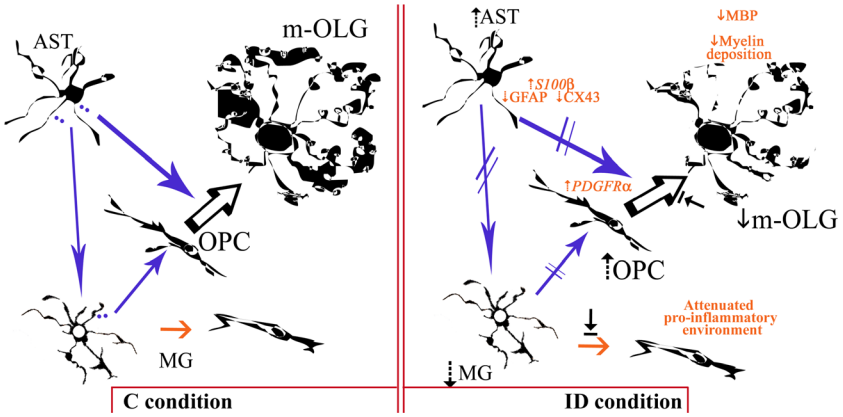

Fig. 9 Schematic illustration showing the effects of ID on glial cells. *OPC* oligodendroglial precursor cell, *m-OLG* mature oligodendrocyte, *AST* astrocyte, *MG* microglialcell, *PDGFRα* platelet-derived growth factor receptor α (OPC marker), *S100β*, *GFAP* glial fibrillary acidic protein, *CX43* connexin 43 (AST markers). The *left panel* illustrates the cross talk involving the three glial cell types during ontogenic myelination in a C animal. The *right panel* represents the same cross talk in an ID animal. *Dotted black arrows* indicate the changing tendencies in glial cell proliferation. *Orange arrows* indicate cellular features associated with ID depicted by marker expression. *Solid black arrow* indicates diminished number of m-OLG, which leads to hypomyelination. *Blue arrows* represent alterations in iron flow involving glial cells. In sum, low iron availability hampers environmental glial cell response, particularly AST, preventing iron delivery to MG and OLG. Overall, ID curbs OLG maturation into m-OLG through mitigated MG and AST responses

our ID animals exhibited CX43 downregulation concurrent with high AST proliferation but no differentiation, it may be speculated that low iron conditions promote AST immaturity, making them unable to participate in OLG differentiation.

During postnatal development, MG represent an important iron source for OLG. It has been shown that MG accumulate iron just before myelination and that the decrease in MG iron load is paralleled by an accumulation of iron in OLG [22]. These findings suggest that MG first accumulate iron and then release it to developing OPC during myelination, when iron requirements are maximal for OPC maturation [8]. Studies on MG iron deprivation demonstrate that an increment in iron concentrations can affect microglial function by enhancing their release of inflammatory molecules. Therefore, iron-loaded LPS-activated MG show increased release of matrix metalloproteinase-9 [59] and pro-inflammatory cytokines TNF-α, and IL-1β [60], as compared to non-iron-loaded LPS-activated MG. In addition, both cytokines induce the synthesis of ferritin, thus contributing to the regulation of iron metabolism [61]. Interestingly, iron chelator deferroxamine inhibits LPS-induced MG activation and the production of pro-inflammatory cytokines [60].

This work further reports differences in MG anti-inflammatory profile in C and ID animals, both at P21 and P35. ID was observed not only to prevent LPS-triggered induction of pro-inflammatory cytokines IL-1β and TNFα but also to increase the expression of IL-10, an anti-inflammatory molecule. IL-1β promotes remyelination in the adult CNS through the induction of AST and MG/macrophage-derived IGF-1 [17]. Our results showing a decrease in IL-1β in ID suggest a cross talk between MG and OLG, probably through the modulation of growth factors involved in the proliferation and maturation of OPC. Overall, our in vivo and in vitro results confirm that gestational ID has profound and long-lasting effects on glial cells. These events are not circumscribed to OLG but extend to AST and MG as well, probably due to the interplay of the different cell types present in the brain to contribute to proper myelin (Fig. 9). Current experiments are now focusing on the characterization of the molecular nature of AST-OLG cross talk in ID conditions, and on the degree of involvement of glial-restricted precursor cells (GRPc) in the initial outcome of ID.

Acknowledgements This work was supported by generous funding from Universidad de Buenos Aires; grant number: 20020100100395. We are especially grateful to Marianela Vence for her special dedication and technical assistance with experimental animals and to María Marta Rancez for her helpful insights.

Compliance with Ethical Standards

Conflict of Interest The authors have no conflict of interest to declare.

References

1. Beard JL (2008) Why iron deficiency is important in infant development. J Nutr 138:2534–2536
2. Lozoff B, Beard J, Connor J, Barbara F, Georgieff M, Schallert T (2006) Long-lasting neural and behavioral effects of iron deficiency in infancy. Nutr Rev 64:S34–S43 discussion S72-91
3. Piñero DJ, Li NQ, Connor JR, Beard JL (2000) Variations in dietary iron alter brain iron metabolism in developing rats. J Nutr 130:254–263
4. Badaracco ME, Ortiz EH, Soto EF, Connor J, Pasquini JM (2008) Effect of transferrin on hypomyelination induced by iron deficiency. J Neurosci Res 86:2663–2673
5. Ray PD, Huang BW, Tsuji Y (2012) Reactive oxygen species (ROS) homeostasis and redox regulation in cellular signaling. Cell Signal 24:981–990

6. Johnstone D, Milward EA (2010) Genome-wide microarray analysis of brain gene expression in mice on a short-term high iron diet. Neurochem Int 56:856–863
7. Meguro R, Asano Y, Odagiri S, Li C, Shoumura K (2008) Cellular and subcellular localizations of nonheme ferric and ferrous iron in the rat brain: a light and electron microscopic study by the perfusion-Perls and -Turnbull methods. Arch Histol Cytol 71: 205–222
8. Todorich B, Pasquini JM, Garcia CI, Paez PM, Connor JR (2009) Oligodendrocytes and myelination: the role of iron. Glia 57:467–478
9. Todorich B, Zhang X, Connor JR (2011) H-ferritin is the major source ofironforoligodendrocytes. Glia 59:927–935
10. Rosato-Siri MV, Badaracco ME, Ortiz EH, Belforte N, Guardia Clausi M, Soto EF, Bernabeu R, Pasquini JM (2010) Oligodendrogenesis in iron-deficient rats: effect of Apotransferrin. J Neurosc Res. 88:1695–1607
11. Forge JK, Pedchenko TV, LeVine SM (1998) Iron deposits in the central nervous system of SJL mice with experimental allergic encephalomyelitis. Life Sci 63:2271–2284
12. Zarruk JG, Berard JL, Passos Dos Santos R, Kroner A, Lee J, Arosio P, David S (2015) Expression of iron homeostasis proteins in the spinal cord in experimental autoimmune encephalomyelitis and their implications for iron accumulation. Neurobiol Dis 81:93–107
13. Clemente D, Ortega MC, Melero-Jerez C, de Castro F (2013) The effect of glia-glia interactions on oligodendrocyte precursor cell biology during development and in demyelinating diseases. Front Cell Neurosci 7:268
14. Zhang SC, Goetz BD, Carré JL, Duncan ID (2001) Reactive microglia in dysmyelination and demyelination. Glia 15:101–109
15. Zhang X, Surguladze N, Slagle-webb B, Cozzi A, Connor JR (2006) Cellular iron status influences the functional relationship between microglia and astrocytes. Glia 54:795–804
16. Albrecht PJ, Murtie JC, Ness JK, Redwine JM, Enterline JR, Armstrong RC, Levison SW (2003) Astrocytes produce CNTF during the remyelination phase of viral-induced spinal cord demyelination to stimulate FGF-2 production. Neurobiol Dis 13:89–101
17. Mason JL, Suzuki K, Chaplin DD, Matsushima GK (2001) Interleukin-1beta promotes repair of the CNS. J Neurosci 21: 7046–7052
18. Gudi V, Skuljec J, Yidiz O, Frichert K, Skripuletz T, Moharregh-Khlabani D, Voss E, Wissel K et al (2011) Spatial and temporal profiles of growth factor expression during CNS demyelination reveal the dynamics of repair priming. PLoS One 6(7):e22623
19. Schulz K, Kroner A, David S (2012) Iron efflux from astrocytes plays a role in remyelination. J Neurosci 32:4841–4847
20. Fischer R, Wajant H, Kontermann R, Pfizenmaier K, Maier O (2014) Astrocyte-specific activation of TNFR2 promotes oligodendrocyte maturation by secretion of leukemia inhibitory factor. Glia 62:272–283
21. Connor JR, Pavlick G, Karli D, Menzies SL, Palmer C (1995) A histochemical study of iron-positive cells in the developing rat brain. J Comp Neurol 355:111–123
22. Cheepsunthorn P, Palmer C, Connor JR (1998) Cellular distribution of ferritin subunits in postnatal rat brain. J Comp Neurol 400:73–86
23. Franco PG, Pasquini LA, Pérez MJ, Rosato-Siri MV, Silvestroff L, Pasquini JM (2015) Paving the way for adequate myelination: the contribution of galectin-3, transferrin and iron. FEBS Lett 589: 3388–3395
24. McCarthy KD, de Vellis J (1980) Preparation of separate astroglial and oligodendroglial cell cultures from rat cerebral tissue. J Cell Biol 85:890–802
25. Miron VE, Boyd A, Zhao JW, Yuen TJ, Ruckh JM, Shadrach JL, van Wijngaarden P, Wagers AJ et al (2013) M2 microglia and macrophages drive oligodendrocyte differentiation during CNS remyelination. Nat Neurosci 16:1211–1218
26. Jiang P, Chen C, Wang R, Chechneva OV, Chung SH, Rao MS, Pleasure DE, Liu Y et al (2013) hESC-derived Olig2+ progenitors generate a subtype of astroglia with protective effects against ischaemic brain injury. Nat Commun 4:2196
27. Valeiras B, Rosato-Siri MV, Codagnone M, Reines A, Pasquini JM (2014) Gender influence on schizophrenia-relevant abnormalities in a cuprizone demyelination model. Glia 62:1629–1644
28. Kiernan JA, Chromoxane cyanine R. I (1984) Physical and chemical properties of the dye and of some of its iron complexes. J Microsc 134:13–23
29. Mirro J, Stass SA (1985) Fluorescent microsphere detection of surface antigens and simultaneous cytochemistries in individual hematopoietic cells. Am J Clin Pathol 83:7–11
30. Rosato Siri MV, Badaracco ME, Pasquini JM (2013) Glatiramer promotes oligodendroglial cell maturation in a cuprizone-induced demyelination model. Neurochem Int 63:10–24
31. Pfaffl MW (2001) A new mathematical model for relative quantification in real-time RT-PCR. Nucleic Acids Res 29:2002–2007
32. Rajasekharan S, Baker KA, Horn KE, Jarjour AA, Antel JP, Kennedy TE (2009) Netrin 1 and dcc regulate oligodendrocyte process branching and membrane extension via Fyn and RhoA. Development 136:415–426
33. Ferreira T, Blackman A, Oyrer J, Jayabal A, Chung A, Watt A, Sjöström J, van Meyel D (2014) Neuronal morphometry directly from bitmap images. Nat Methods 11:982–984
34. Zhang Y, Chen K, Sloan SA, Bennett ML, Scholze AR, O'Keeffe S, Phatnani HP, Guarnieri P et al (2014) An RNA-sequencing Transcriptome and splicing database of glia, neurons, and vascular cells of the cerebral cortex. The J of Neurosc 34:11929–11947
35. Crain JM, Nikodemova M, Watters JJ (2013) Microglia express distinct M1 and M2 phenotypic markers in the postnatal and adult central nervous system in male and female mice. J Neurosci Res 91(9):1143–1151
36. Nualart-Marti A, Solsona C, Douglas FR (2013) Gap junction communication in myelinating glia. Review. Biochim and Biophys Acta 1828:69–78
37. Kwik-Uribe CL, Golub MS, Keen CL (2000) Chronic marginal iron intakes during early development in mice alter brain iron concentrations and behavior despite postnatal iron supplementation. J Nutr 130:2040–2048
38. Lozoff B (2000) Perinatal iron deficiency and the developing brain. Pediatr Res 48:137–139
39. Ortiz E, Pasquini JM, Thompson K, Felt B, Butkus G, Beard J, Connor JR (2004) Effect of manipulation of iron storage, transport, or availability on myelin composition and brain iron content in three different animal models. J Neurosc Res 77:681–689
40. Rao R, Tkac I, Unger EL, Ennis K, Hurst A, Schallert T, Connor J, Felt B et al (2013) The iron supplementation dose for perinatal iron deficiency differentially alters the neurochemistry of frontal cortex and hippocampus in adult rats. Pediatr Res 73:31–37
41. Lozoff B, Georgieff MK (2006) Iron deficiency and brain development. Semin Pediatr Neurol 13:158–165
42. Georgieff MK (2008) The role of iron in neurodevelopment: fetal iron deficiency and the developing hippocampus. Biochem Soc Trans 36:1267–1271
43. Greminger AR, Mayer-Pröschel M (2015) Identifying the threshold of iron deficiency in the central nervous system of the rat by the auditory brainstem response. ASN Neuro 7:1–10
44. Harvey L, BoksaP (2014) Additive effects of maternal iron deficiency and prenatal immune activation on adult behaviors in rat offspring. Brain Behav Immun 40:27–37
45. Badaracco ME, Siri MV, Pasquini JM (2010) Oligodendrogenesis: the role of iron. Biofactors 36:98–102

46. Morath DJ, Mayer-Proschel M (2002) Iron deficiency during embryogenesis and consequences for oligodendrocyte generation in vivo. Dev Neurosci 24:197–107
47. Stefanović D, Stefanović M, Lalošević D (2015) Use of eriochrome cyanine R in routine histology and histopathology: is it time to say goodbye to hematoxylin? Biotech Histochem 90:461–469
48. Noble M, Smith J, Power J, Mayer-Pröschel M (2003) Redox state as a central modulator of precursor cell function. Ann N Y Acad Sci 991:251–271
49. Huang S, Du F, Li L, Liu Y, Liu Y, Zhang C, Qian ZM (2014) Angiotensin II inhibits uptake of transferrin-bound iron but not non-transferrin-bound iron by cultured astrocytes. Neuropeptides 48:161–166
50. Simpson IA, Ponnuru P, Klinger ME, Myers RL, Devraj K, Coe CL, Lubach GR, Carruthers A et al (2015) A novel model for brain iron uptake: introducing the concept of regulation. J Cereb Blood Flow Metab 35:48–57
51. Miyamoto N, Maki T, Shindo A, Liang AC, Maeda M, Egawa N, Itoh K, Lo EK et al (2015) Astrocytes promote Oligodendrogenesis after white matter damage via brain-derived Neurotrophic factor. J Neurosci 35:14002–14008
52. Jeong SY, David S (2003) Glycosyl phosphatidyl inositol-anchored ceruloplasmin is required for iron efflux from cells in the central nervous system. J Biol Chem 278:27144–27148
53. Arnett HA, Mason J, Marino M, Suzuki K, Matsushima GK, Ting JP (2001) TNF alpha promotes proliferation of oligodendrocyte progenitors and remyelination. Nat Neurosci 4:1116–1122
54. Messersmith DJ, Murtie JC, Le TQ, Frost EE, Armstrong RC (2000) Fibroblast growth factor 2 (FGF2) and FGF receptor expression in an experimental demyelinating disease with extensive remyelination. JNeurosci Res 62:241–256
55. Hinks GL, Franklin RJ (1999) Distinctive patterns of PDGF-A, FGF-2, IGF-I, and TGF-beta1 gene expression during remyelination of experimentally-induced spinal cord demyelination. Mol Cell Neurosci 14:153–168
56. Fernandez LL, de Lima MN, Scalco F, Vedana G, Miwa C, Hilbig A, Vianna M, Schröder N (2011) Early post-natal iron administration induces astroglial response in the brain of adult and aged rats. Neurotox Res 20:193–199
57. Homkajorn B, Sims NR, Muyderman H (2010) Connexin 43 regulates astrocytic migration and proliferation in response to injury. Neurosci Lett 486:197–201
58. Szajkowski R, Friel JK, Diehl-Jones W, Valdimarsson G (2006) Effects of iron and oxidative stress on Cx43 expression and phosphorylation. FASEB J 20:A617
59. Mairuae N, Connor JR, Cheepsunthorn P (2011) Increased cellular iron levels affect matrix metalloproteinase expression and phagocytosis in activated microglia. Neurosci Lett 500:36–40
60. Zhang X-Y, Cao J-B, Zhang L-M, Li Y-F, Mi W-D (2015) Deferoxamine attenuates lipopolysaccharide-induced neuroinflammation and memory impairment in mice. J Neuroinflammation 12: 20
61. Rogers JT (1996) Ferritin translation by interleukin-1and interleukin-6: the role of sequences upstream of the start codons of the heavy and light subunit genes. Blood 87:2525–2537